

# Weak thermal reduction of biphase Fe<sub>2</sub>O<sub>3</sub>(0001) films grown on Pt(111): sub-surface Fe<sup>2+</sup> formation

Hengshan Qiu<sup>a,1</sup>, Volker Staemmler<sup>b</sup>, Helmut Kühlenbeck<sup>a,\*</sup>, Ernst Bauer<sup>c</sup>, Hans-Joachim Freund<sup>a</sup>

<sup>a</sup>Fritz-Haber-Institut der Max-Planck-Gesellschaft, Faradayweg 4-6, D-14195 Berlin, Germany

<sup>b</sup>Lehrstuhl für Theoretische Chemie, Ruhr-Universität Bochum, D-44780 Bochum, Germany

<sup>c</sup>Department of Physics, Arizona State University, 85287, Tempe, USA

## Abstract

The initial thermal reduction of biphase Fe<sub>2</sub>O<sub>3</sub>(0001) films grown on Pt(111) has been studied with HREELS, LEED, TDS, and synchrotron-based valence band photoelectron spectroscopy. *Ab initio* calculations of the electronic excitation energies of Fe<sup>2+</sup> and Fe<sup>3+</sup> ions in different oxidic environments were carried out to support the experimental studies. Annealing the biphase Fe<sub>2</sub>O<sub>3</sub>(0001) at 1000 K results in the desorption of oxygen and a concomitant

---

<sup>1</sup>Present Address: Laboratory of Environmental Sciences and Technology, Xinjiang Technical Institute of Physics and Chemistry, Chinese Academy of Sciences, Urumqi, Xinjiang 830011, China.

\*Corresponding Author: Email: [kuhlenbeck@fhi-berlin.mpg.de](mailto:kuhlenbeck@fhi-berlin.mpg.de), tel: +49 30 8413 4222, fax: +49 30 8413 4307

significant change of the electronic excitation spectra measured with HREELS. On the other hand, studies employing more surface sensitive methods like LEED, vibrational spectroscopy of adsorbates, and surface-sensitive valence band photoelectron spectroscopy reveal barely any changes induced by the desorption of oxygen. Based on these experimental findings we propose that the thermal reduction of biphasic  $\text{Fe}_2\text{O}_3(0001)$  occurs mostly below the surface under the chosen conditions.

*Keywords:*  $\text{Fe}_2\text{O}_3(0001)$ , biphasic, reduction, electronic excitations, HREELS, *ab initio* calculations

## 1. Introduction

The rich phase diagram of iron oxides with the oxide phases  $\text{FeO}$ ,  $\text{Fe}_3\text{O}_4$ ,  $\alpha\text{-Fe}_2\text{O}_3$  and the artificially synthesized  $\gamma\text{-Fe}_2\text{O}_3$  and  $\varepsilon\text{-Fe}_2\text{O}_3$  phases as well as corrosion processes and the applications of iron oxides in catalysis, photoelectrochemistry and magnetic recording etc. have attracted considerable scientific interest towards these oxides [1-9].  $\alpha\text{-Fe}_2\text{O}_3$  is the thermodynamically most stable phase of the Fe-O system under ambient conditions, and the most common form in nature [1, 10]. Its (0001) surface exhibits a rather complicated T-P( $\text{O}_2$ ) surface phase diagram [1, 8, 10-12]: oxygen termination, Fe termination, mixed oxygen and iron termination [13, 14],  $\text{Fe}_3\text{O}_4$  termination [15-17],  $\text{Fe}_{1-x}\text{O}$  termination [17], termination by an ordered array of  $\text{FeO}_{1-x}$  and  $\text{Fe}_2\text{O}_3$  patches [18], termination by an ordered array of  $\text{FeO}(111)$ , Fe- and O-terminated  $\text{Fe}_2\text{O}_3(0001)$  patches [19], and ferryl termination [20] were reported. Surface polarity may introduce additional complexity since it must be compensated by structural/electronic modifications [21, 22].

If the oxide is prepared under not too high oxygen pressures, a complex LEED pattern with a manifold of hexagonally arranged spots distributed around the positions of the regular  $\text{Fe}_2\text{O}_3(0001)$  (1x1) LEED spots may be observed. This was first observed by Lad and Henrich [17], who attributed the observed LEED pattern to multiple scattering between a  $\text{Fe}_{1-x}\text{O}$  surface layer and regular  $\text{Fe}_2\text{O}_3(0001)$  below this layer. Later STM studies found an ordered array of patches of two different structures which were identified as  $\text{FeO}_{1-x}(111)$  and  $\text{Fe}_2\text{O}_3(0001)$  [18]. Hereafter this surface termination was named biphasic structure. In a later investigation Lanier et al [16] questioned these results, and instead attributed the biphasic structure to a  $\text{Fe}_3\text{O}_4(111)$ -derived overlayer on  $\text{Fe}_2\text{O}_3(0001)$ . This issue has not yet been settled, but it is well accepted that the surface termination of  $\text{Fe}_2\text{O}_3(0001)$  depends closely on environmental parameters such as temperature and gas atmosphere [8, 9, 12, 13, 23-29].

The main method employed in this study was high resolution electron energy loss spectroscopy (HREELS) which was used in the regimes of vibrational and electronic excitations. Especially the electronic excitations within the Fe3d shell are characteristic for the Fe oxidation state and therefore their study was expected to give additional hints towards the nature of the biphasic structure. Having follow-up studies of catalytic properties in mind, also the modification of the surface electronic and geometric structure upon annealing was investigated.

## **2. Experimental**

HREELS, low energy electron diffraction (LEED), thermal desorption spectroscopy (TDS), and synchrotron-based valence band spectroscopy were employed in this study. The UHV

apparatus used for HREELS, LEED, and TDS consists of a preparation chamber and a HREELS analysis chamber separated by a gate valve. The preparation chamber is equipped with an Ar ion sputter gun for sample cleaning, an iron evaporator with e-beam heating for film preparation, a LEED/AES module (SPECS, Germany), and a quadrupole mass spectrometer (Hiden, UK) for TDS experiments. The iron rod used as evaporant in the evaporator had a purity of 99.995%, and the deposition rate was calibrated in-situ by a quartz microbalance mounted on the manipulator at a fixed position of about 10 cm above the sample. The HREELS chamber houses a HREEL spectrometer (Delta 0.5 from VSI) with an ultimate energy resolution better than 1 meV. The primary energy of the electron beam was set to 40 eV or 8 eV for the study of electronic or vibrational excitations, respectively. The incident angle for specular detection was set to 55° relative to the surface normal, while for off-specular electron detection the energy analyzer was rotated by 10° to a larger detection angle in the scattering plane. Spectra in off-specular geometry were recorded without readjustment of the electron optics of the HREELS spectrometer. The base pressure in the preparation chamber was better than  $2 \times 10^{-10}$  mbar, and in the HREELS chamber it was  $5 \times 10^{-11}$  mbar. A Pt(111) sample ( $7 \times 8 \times 2$  mm<sup>3</sup>) was mounted on a transferable sample plate with a K-type thermocouple spot-welded to the side of the sample. The sample temperature could be varied from 90 K (with liquid nitrogen cooling) to 1300 K (with electron bombardment heating). Throughout the experiments we always used a doser for gas dosing and film oxidation, which can effectively reduce the background pressure by a factor of about 50. The doser consists of a stainless steel tube with a diameter of ~1 cm, which during dosing is positioned such that it ends at a distance of a few mm in front of the sample surface. A 50 μm pinhole is mounted at the beginning of the tube. Therefore the pressure in the gas handling system during dosing is significantly higher than the pressure at the sample surface which reduces the level of gas contamination resulting

from gases adsorbed on the inner walls of the gas inlet system. The “monolayer (ML)” unit used in this work is defined as one atom per 2D surface unit cell of Pt(111) which amounts to an atomic density of  $1.51 \times 10^{15}$  atoms/cm<sup>2</sup>.

Valence band photoelectron spectra were measured at the UE52-PGM beam line of the electron storage ring of the Helmholtz center in Berlin (formerly called BESSY II), Germany, using the sample and the manipulator of the HREELS system. The pressure of the background gas atmosphere was better than  $1.0 \times 10^{-9}$  mbar in the preparation chamber and about  $5.0 \times 10^{-10}$  mbar in the spectroscopy chamber. The latter is equipped with a hemispherical electron energy analyzer (R4000, VG Scienta) for photoelectron spectroscopy. Spectra of the Pt 4f line were recorded in order to calibrate the photon energy. The spectra presented in this manuscript were all measured with 120 eV photons at an electron emission angle of 80° with respect to the surface normal, which results in a vertical electron escape depth of only about 1 Å as estimated using a mean free electron path length computed with the Quases IMFP program [30]. Thus, most of the intensity in these spectra stems from the topmost layer. Some spectra were also taken at normal emission to look somewhat deeper in the surface layer.

The Pt(111) substrate was cleaned by repeated cycles of sputtering (with an ion current of about 10 µA for 30 minutes) followed by annealing at 1300 K for 10 minutes. Surface cleanliness and order were checked with Auger electron spectroscopy and LEED, respectively.

Well-established preparation procedures are reported for iron oxide layers on Pt(111) [31]. These procedures were adopted for the preparation of the samples investigated in this study. Thin layers have a crucial advantage over single crystals for the case of electrically insulating materials: experimental methods involving charged particles can be applied since the layers do not charge if they are not thicker than (typically) a few nanometers [32].

1 ML thick FeO(111) layers were prepared on Pt(111) by oxidizing 1 ML Fe at 1000 K for 2 minutes in  $1.0 \times 10^{-6}$  mbar of O<sub>2</sub>. Fe<sub>2</sub>O<sub>3</sub> layers were grown on such a FeO layer by four cycles of deposition of 8 ML Fe followed by an oxidation treatment. For biphasic Fe<sub>2</sub>O<sub>3</sub> the oxidation was performed at 1050 K in  $1.0 \times 10^{-5}$  mbar to  $5.0 \times 10^{-5}$  mbar of O<sub>2</sub>. Regular Fe<sub>2</sub>O<sub>3</sub>(0001) (1x1) was prepared by oxidation of a layer with biphasic termination at 1050 K in 2 mbar of oxygen for 5 min. To this end the sample was transferred into a dedicated high-pressure cell which could be separated from the experimental chamber via a gate valve. This procedure resulted reproducibly in a slight Mo contamination of the oxide layer seen in the differentiated AES spectra recorded with the LEED system. Electronic and vibrational HREELS spectra did not show any special structures in the band gap nor were indications of the MoO<sub>3</sub> band gap visible. Therefore the slight contamination was not taken into account in the data analysis, but should be kept in mind.

For all oxidation processes, the heating rate was 2 K/s, and the oxygen supply was switched on already before the heating step started and switched off during cool-down when the sample had reached a temperature of 500 K [31]. For studies of reduced biphasic Fe<sub>2</sub>O<sub>3</sub> the layer was annealed at 1000 K in vacuum for 5 minutes. Layers prepared in this way will be called *O-poor* in the following, while non-reduced layers will be called *O-rich*.

### **3. *Ab initio* cluster calculations**

A series of quantum chemical embedded cluster calculations for the low-lying electronic states of the iron oxides was performed in order to provide additional information for the interpretation of the electronic HREELS spectra. We have considered Fe<sup>3+</sup> and Fe<sup>2+</sup> ions in two

different crystal environments, in the cubic rock-salt structure of FeO (wuestite) [33] and in the corundum-type structure of  $\alpha$ -Fe<sub>2</sub>O<sub>3</sub> [33], each time both in the bulk and at the surface, to check the influence of the local environment on the calculated excitation energies. The clusters and the embedding point charge fields were designed as described before [34, 35].

All clusters consisted of one central Fe atom surrounded by one shell of adjacent O atoms, six for bulk Fe atoms and five or three for Fe atoms at the FeO(001) and Fe<sub>2</sub>O<sub>3</sub>(0001) surface, respectively. These clusters were embedded in large point charge fields to simulate the correct electrostatic environment. The point charges had ionicities of +2 (FeO) or +3 (Fe<sub>2</sub>O<sub>3</sub>) and -2 and were placed at the lattice points of the respective ideal crystals. In order to prevent the electrons of the clusters from floating towards the point charge field, all positive point charges directly bound to one of the O atoms of the cluster were equipped with repulsive pseudo potentials. The Ni<sup>2+</sup> large-core pseudo potential of the Stuttgart group [36] was used for this purpose.

All calculations were performed by means of wavefunction based *ab initio* methods using the Bochum open-shell programs, in particular the SCF, CAS-SCF and CI parts of this package [37-39]. Two computational steps were necessary for each crystal structure and each oxidation state of the Fe atoms. In the first step molecular orbitals have to be determined, either by a SCF (more precisely, a restricted open-shell Hartree-Fock, ROHF) or a CAS-SCF (complete active space SCF) calculation. These orbitals are then used in the subsequent CAS-CI (configuration interaction) step for calculating the excitation energies.

In the gas phase, the ground state of a Fe<sup>3+</sup> ion is a non-degenerate <sup>6</sup>S state with the configuration 3d<sup>5</sup>. The lowest excitation energy to the first excited state, which is a highly degenerate <sup>4</sup>G state with the same 3d<sup>5</sup> configuration, is as large as 3.998 eV [40]. The ground

state of a  $\text{Fe}^{2+}$  ion, on the other hand, is a five-fold spatially degenerate  $^5\text{D}$  state with the configuration  $3\text{d}^6$ . Its lowest excited states,  $^3\text{P}$  and  $^3\text{H}$ , belong to the same  $3\text{d}^6$  configuration and are by about 2.5 eV higher in energy. In a crystal field, the degeneracies of the excited  $^4\text{G}$  state of  $\text{Fe}^{3+}$  and of the  $^5\text{D}$  ground state of  $\text{Fe}^{2+}$  are partially or fully removed. Since the ligand field strength of  $\text{O}^{2-}$  anions is in the order of 1.0 eV, one can expect that the lowest d-d excitation energy of a  $\text{Fe}^{3+}$  cation is reduced in oxide environments from 4.0 to about 3.0 eV. Similarly, the splitting of the  $^5\text{D}$  ground state of  $\text{Fe}^{2+}$  into a lower  $^5\text{T}_{2g}$  and a higher  $^5\text{E}_g$  state in octahedral symmetry will also be in the order of 1.0 eV.

The results of our calculations as given in the Tables 1 ( $\text{Fe}^{3+}$ ) and 2 ( $\text{Fe}^{2+}$ ) confirm these expectations. The lowest excitation energy of  $\text{Fe}^{3+}$  (Table 1) is always between about 3.0 and 3.7 eV, both for bulk and surface environments. This means that it is in all cases larger than the band gaps of  $\text{FeO}$  and  $\text{Fe}_2\text{O}_3$ . When the ligand field strength is increased, e.g. by artificially shortening the Fe-O distance from its value of 2.16 Å in the  $\text{FeO}$  crystal to 2.02 Å, the excitation energy is getting smaller; at the  $\text{Fe}_2\text{O}_3(0001)$  surface, on the other hand, the  $\text{Fe}^{3+}$  ion is only three-fold coordinated and therefore the ligand field strength is smaller and the excitation energy larger than in the bulk. The calculated splitting of the  $^5\text{D}$  level of the  $\text{Fe}^{2+}$  ion (Table 2) is about 1.2 eV for bulk  $\text{FeO}$  (2.08 Å) and  $\text{Fe}_2\text{O}_3$ , i.e. for  $\text{Fe}^{2+}$  ions the lowest excitation energy lies in the band gap. At the surface the degeneracy of the  $^5\text{D}$  state is further reduced. For the  $\text{Fe}_2\text{O}_3(0001)$  surface the transition to the highest component of  $^5\text{D}$ , at 1.09 eV, is spin allowed and also weakly dipole allowed whereas all other transitions are either spin or dipole forbidden or both. It is well known [1, 7, 12] that the Fe cations at the  $\text{Fe}_2\text{O}_3(0001)$  surface are pulled slightly inwards towards the first oxygen layer. Allowing for this relaxation we found that the distance between the Fe atom and the next O atoms shrinks from 1.96 to about 1.80

Å. (The precise amount of this relaxation depends to some extent on the cluster setup and further details of the calculations.) The excitation energy of the allowed transition of the Fe<sup>2+</sup> cation in this position is increased from 1.09 to about 1.50 eV.

All calculated excitation energies correspond to local d-d excitations of the Fe<sup>3+</sup> and Fe<sup>2+</sup> ions in the respective crystal fields. By extending the active space in the CAS-CI calculations we checked whether charge-transfer excitations, in particular ligand-to-metal charge-transfer, might be important, but none of the excitation energies presented in the tables is modified substantially and no additional low-lying charge-transfer states could be detected in the energy range below 2.0 eV. Of course, band structure effects, e.g. reasonable values for band gaps cannot be obtained by the present calculations employing rather small clusters.

## 4. Results and discussions

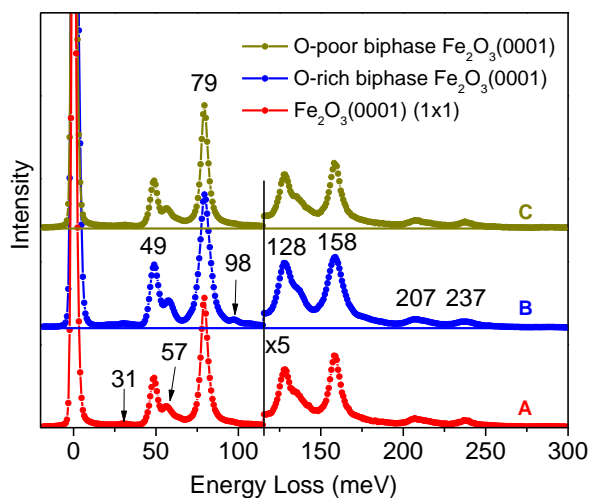
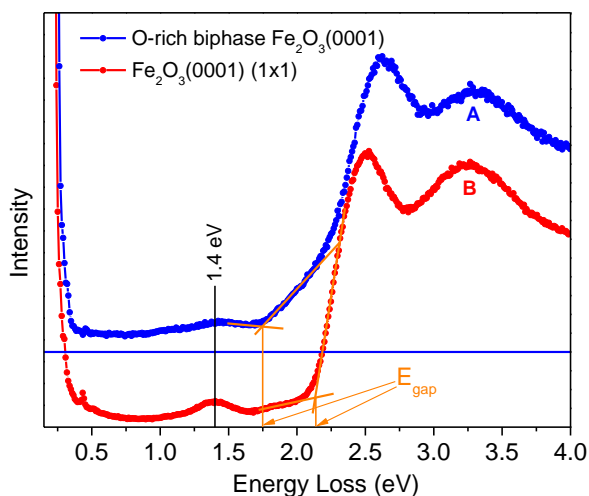


Figure 1: Electronic excitation spectra of regular  $\text{Fe}_2\text{O}_3(0001)$  (1x1) (A) and biphas  $\text{Fe}_2\text{O}_3$  (B). Both spectra were taken in specular geometry. The spectra are normalized such that the peaks at  $\sim 3.3$  eV have equal intensities. Approximate gap energies are indicated. They are constructed from the intersection of lines representing approximations to the intensity in the gap and the increasing intensity beyond the gap.

Figure 2: Vibrational HREELS spectra of *O-rich* and *O-poor* biphas  $\text{Fe}_2\text{O}_3(0001)$  and  $\text{Fe}_2\text{O}_3(0001)$  (1x1). The spectra were recorded in specular geometry and normalized such that the losses at 79 meV have equal intensities.

Figure 1-A displays HREELS spectra of regular  $\text{Fe}_2\text{O}_3(0001)$ -(1x1) on Pt(111) for an energy range up to 4 eV which is dominated by electronic excitations.  $\text{Fe}_2\text{O}_3$  is a semiconductor with experimentally determined values for the band gap width ranging from 2.0 eV to 2.25 eV [22, 41, 42]. First principle calculations with the GGA+U approximation gave a bulk band gap of about 2.0 eV [7]. The value of  $\sim 2.15$  eV shown in Figure 1-A agrees with these results. There are no electronic states in the bulk band gap of  $\text{Fe}_2\text{O}_3$ , neither in the cluster calculations (Table 1) nor in the band structure calculations with the GGA+U approximation [7]. It is known that the latter method is good for bulk properties while surface properties are described better with the pure GGA approximation. A theoretical study employing GGA calculations did not

give a band gap in the surface region [7], which might indicate that the loss intensity in the band gap seen in Figure 1 originates in the surface region. However, defect states in the bulk and at the surface may also contribute.

The phonon spectrum of  $\text{Fe}_2\text{O}_3(0001)-(1\times 1)$  in Figure 2-A shows loss peaks at 31, 49, 57, 79, 98, 128, 158, 207 and 237 meV. The loss peaks at 31, 49, 57 and 79 meV are due to single excitations of bulk optical phonons (Fuchs-Kliewer phonons), and the remaining peaks are multiple excitations of these phonons [43, 44].

Figure 1 shows that the loss feature at 1.4 eV in the band gap is not only present for regular  $\text{Fe}_2\text{O}_3(0001) (1\times 1)$  but also for the biphasic. The overall intensity in the gap of the biphasic is somewhat higher, which can be attributed to a somewhat lower average oxidation state. In particular, the lower oxidation state may be responsible for the strong intensity increase above  $\sim 1.75$  eV in Figure 1-A. Assuming that the states above  $\sim 1.75$  eV in Figure 1-A are due to optically allowed transitions one would get a surface band gap of  $\sim 1.75$  eV for the biphasic as indicated in the figure.

Transitions of  $\text{Fe}^{3+}$  ions do not exist in the energy range of the gap according to the cluster calculations (Table 1). For  $\text{Fe}^{2+}$  ions, on the other hand, bulk transitions (Table 2a) as well as surface transitions (Table 2b) are to be expected. The tables give an overview of the d-d transitions of the  $\text{Fe}^{2+}$  ions. The band structure calculations show no gap in the surface region but a surface termination-dependent density of states [7] with an average charge of 2.26 on the Fe ions.

The Fuchs-Kliewer phonon spectra in Figure 2 reveal barely any differences between the spectra of the *O-poor* biphasic, the *O-rich* biphasic and  $(1\times 1) \text{Fe}_2\text{O}_3(0001)$ , which demonstrates

that the structural differences between these system are small in the bulk, which is compatible with the common view that the biphasic is essentially a surface structure.

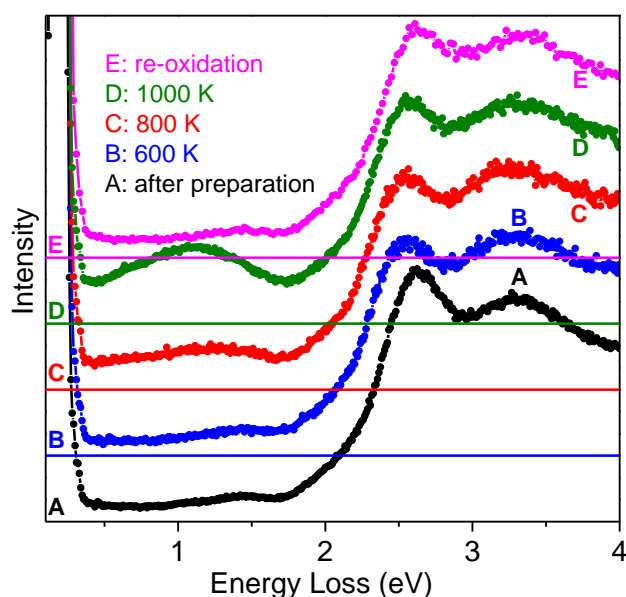


Figure 3: Electronic excitation spectra recorded in specular geometry of (A) an as-prepared  $\text{Fe}_2\text{O}_3$  film and spectra obtained after a subsequent short flash to 600 K (B), 800 K (C), 1000 K (D) and a final re-oxidation step (E). The spectra are normalized such that the state at  $\sim 3.3$  eV has the same intensity in all spectra. For clarity the curves are plotted with a constant y offset between successive graphs; the zero lines are shown and labelled with the label of the respective spectrum.

In order to understand the effect of reduction we have studied the influence of annealing. Figure 3 presents electronic excitation spectra of biphasic  $\text{Fe}_2\text{O}_3$  film recorded directly after preparation [curve A], after annealing at different temperatures [curves B-D], and after oxygen treatment ( $5.0 \times 10^{-5}$  mbar oxygen at 1050 K for 5 min) [curve E]. The most obvious difference between the spectra is that the intensity in the band gap regime increases upon annealing and that treatment with oxygen re-establishes the as-prepared state. Annealing has little influence on the band gap size – it changes by at most 0.1 eV – but strongly affects the intensity of the features in the band gap, which get more intense at about 800 K, accompanied by a shift of the maximum to lower energies. We attribute the temperature-dependent change of the spectra to a variation of the oxygen concentration. This is in agreement with the band

structure calculations, which show a clear decrease of the joint density of states in the surface region with increasing oxygen concentration [7].

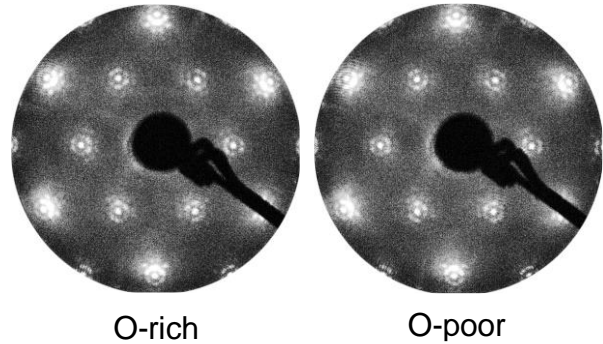
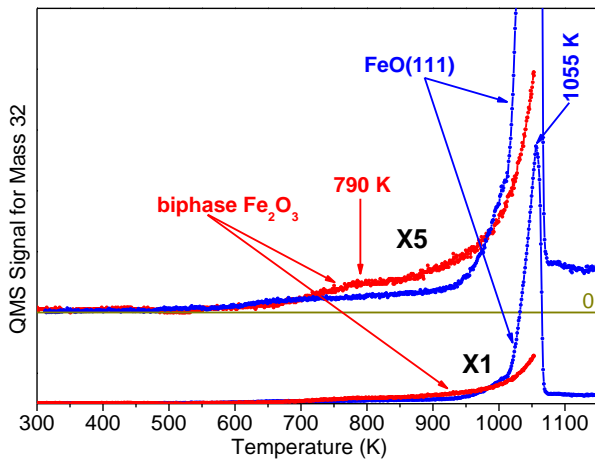


Figure 4: TDS spectra ( $m/e=32$ ,  $O_2$ ) of 1 ML FeO(111) on Pt(111) and freshly prepared  $Fe_2O_3$  with biphasic termination. The heating rate was 1.5 K/s. The upper panel displays the spectra on an expanded (5x) ordinate scale; the zero intensity line is shown below the curves.

Figure 5: LEED patterns of *O-rich* and *O-poor* biphasic  $Fe_2O_3$  films, respectively. The electron energy used in the LEED experiments was 66 eV.

Thermal desorption spectroscopy was employed in order to verify this assumption. Figure 4 shows spectra of 1 ML FeO(111) and a freshly prepared biphasic  $Fe_2O_3$  film. Several masses were monitored, but only  $O_2$  desorption at  $m/e=32$  was detected. The FeO(111) spectrum is very similar to the one published by Sun et al [45], but with the desorption peak maximum shifted by 115 K to lower temperature. We tentatively attribute this to differences in the temperature measurement setup.

The oxygen desorption is related to an oxygen loss in the samples which leads to the strong intensity increase in the band gap in Figure 3 for the biphasic-terminated  $Fe_2O_3$ . Especially at high temperature also desorption of oxygen from the sample holder which warms up during sample heating may contribute to the intensities shown in Figure 4. We assume that this

contribution is rather limited, since the pumped housing of the QMS with the small entrance opening positioned directly in front of the sample surface significantly reduces the probability that molecules desorbing from the sample holder reach the QMS ionizer. Below 1000 K only a weak and broad oxygen desorption peak at 790 K on the steadily rising background can be seen for biphase-terminated  $\text{Fe}_2\text{O}_3$  in Figure 4. This desorption signal correlates well with the significant intensity increase of the feature in the band gap in Figure 3 after annealing at 800 K.

LEED patterns of *O-rich* and *O-poor*  $\text{Fe}_2\text{O}_3$  surfaces are displayed in Figure 5. The floret-like satellites superimposed on the hexagonal structure are typical for biphase  $\text{Fe}_2\text{O}_3(0001)$  [18, 23]. Inspection of the two LEED patterns does not reveal any clear differences regarding the background intensity, the sharpness, and the relative intensities of the diffraction spots, which means that both surfaces have very similar surface structures. However, the different intensities of the band gap states (see Figure 3) and the oxygen desorption peak (see Figure 4) clearly demonstrate that annealing modifies the oxide layer. Thus, the LEED and the HREELS/TDS data are seemingly at variance, which is a consequence of the different surface sensitivities of these methods as will be discussed below.

In HREELS experiments, the interaction of electrons with a solid surface involves two kinds of mechanisms, dipole scattering and impact scattering [43]. The electrons scattered by the dipole scattering mechanism are confined in a narrow spatial angle near to the specular direction while electrons scattered by the impact scattering mechanism usually have a wide angular distribution [43]. Therefore loss spectra collected in specular geometry are usually dominated by dipole-scattered electrons while electrons which have undergone impact scattering are usually dominant at off-specular geometry. Another difference between the impact and the dipole scattering mechanisms is that the surface sensitivities are usually

different. The impact scattering mechanism requires direct interaction of the incoming electrons with the target such that the surface sensitivity is governed by the inelastic mean free electron path (IMFP) while for dipole scattering the penetration depth of the electric field is the relevant length and this is usually much larger than the IMFP for low energy electrons, especially for excitations in the band gap of semiconductors and insulators. Thus dipole-scattering loss peaks in an HREEL spectrum recorded in specular geometry contain information mainly from deeper layers and less from the sample surface. On the other hand, spectra recorded in off-specular geometry, where the dipole scattering cross section is small, contain more information from the surface and surface-near layers since they are usually dominated by impact-scattered electrons.

An estimate for the probing depth of impact scattering may easily be obtained from the IMFP of electrons in  $\text{Fe}_2\text{O}_3$ . The IMFP universal curve [46] indicates (in agreement with the Quases IMFP program [30]) that the IMFP is between about 4 and 10 Å for a kinetic energy of 40 eV. Path lengths between 4 and 10 Å in the solid corresponds to probing depths between 1.1 and 2.9 Å for specular scattering with an incidence angle of  $55^\circ$  with respect to the surface normal. Thus, for impact scattering in specular geometry about 63 % of the intensity stem from a surface layer with such a thickness. The impact-scattering probing depth for the off-specular geometry is similar since the detection angle was varied by only  $10^\circ$ .

In contrast, the probing depth of dipole scattering is significantly larger than that of impact scattering. This is illustrated by experiments performed by Swiderek and coworkers [47]. These authors have investigated the probing depth of dipole scattering by recording HREELS spectra in specular geometry of an ethylene layer covered by argon layers of different thickness. They found that 34 Å of argon damped the intensity of a dipole-allowed loss of

ethylene to approximately 1/3. These numbers may serve as an indication that the probing depth of dipole scattering is indeed significantly larger than that of impact scattering.

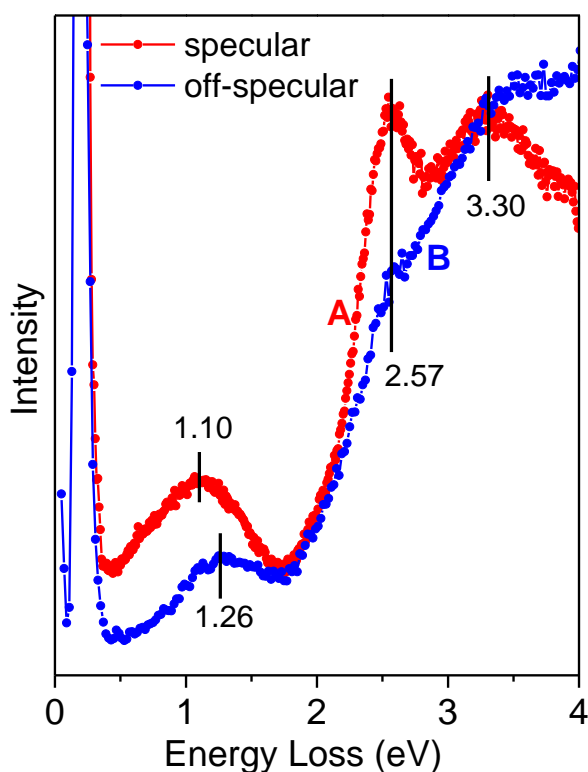


Figure 6: Electronic excitation spectra of *O-poor* biphasic  $\text{Fe}_2\text{O}_3$  recorded in specular (curve A) and  $10^\circ$  off-specular (curve B) geometry. The two spectra were normalized such that the loss peak at 3.30 eV has equal intensity in both spectra.

To exploit the different surface sensitivities and selection rules at specular and off-specular detection angles, we have performed off-specular HREELS measurements. Figure 6 compares spectra of *O-poor* biphasic  $\text{Fe}_2\text{O}_3(0001)$  recorded in specular and off-specular geometry. The off-specular spectrum contains little information from the bulk, since impact-scattering is the dominating loss mechanism in this geometry with most of the intensity coming from the first few layers. The loss peak at 1.26 eV in the  $\text{Fe}_2\text{O}_3$  band gap is therefore attributed to an excitation occurring in the near-surface region.

The peak at 1.10 eV has a pronounced intensity maximum in specular scattering direction, which is a clear indication that the corresponding transition is dipole-allowed. The specular intensity maximum is even more pronounced than that of the dipole-allowed transitions above the band gap energy, which may be attributed to the energy dependence of the angular distribution of inelastically scattered electrons in dipole scattering, which gives a more pronounced near-specular intensity maximum for smaller loss energies [48, 49].

For the energy range of the experimentally observed losses in the band gap, tables 2a and 2b list transitions at 1.15 and 1.09 eV for  $\text{Fe}^{2+}$  in the  $\text{Fe}_2\text{O}_3$  bulk and at the regular  $\text{Fe}_2\text{O}_3(0001)$  surface, respectively. The only dipole-allowed transition among the computed ones is the surface transition at 1.09 eV, which might be related to the dipole-allowed loss at 1.10 eV in Figure 6. The biphasic surface structure is expected to differ somewhat from the structure of the regular  $\text{Fe}_2\text{O}_3(0001)$  surface, and therefore different Fe-O nearest-neighbor distances will probably exist in the biphasic. As discussed before, the energy of the surface transition at 1.09 eV depends on the Fe-O nearest-neighbor distance. Its energy increases to 1.50 eV for a reduction of the Fe-O nearest-neighbor distance from 1.96 to about 1.80 Å. Considering this, also the peak at 1.26 eV in Figure 6 falls into the range of energies covered by this transition. However, we note that  $\text{Fe}^{2+}$ -related charge-transfer transitions, which were not considered in this discussion, may be also expected in the gap.

In order to check the assumption that the reduced iron ions prefer a location below the surface, we have carried out synchrotron-based valence band photoemission measurements. Figure 7 presents highly surface-sensitive spectra of *O-rich* and *O-poor*  $\text{Fe}_2\text{O}_3$  surfaces which were recorded with 120 eV photons at a grazing electron exit angle of  $80^\circ$ . The two spectra in Figure 7 exhibit very similar features, both comprising emission from the hybridized Fe3d and

O2p levels with binding energies between 0 and 10 eV, and a broad feature at 13.4 eV. The peak at 13.4 eV was observed in a previous study and attributed to an unscreened final state ( $3d^4$ ) [50, 51], although other researchers claimed that it could also be an artifact of the chosen calculation method [52].

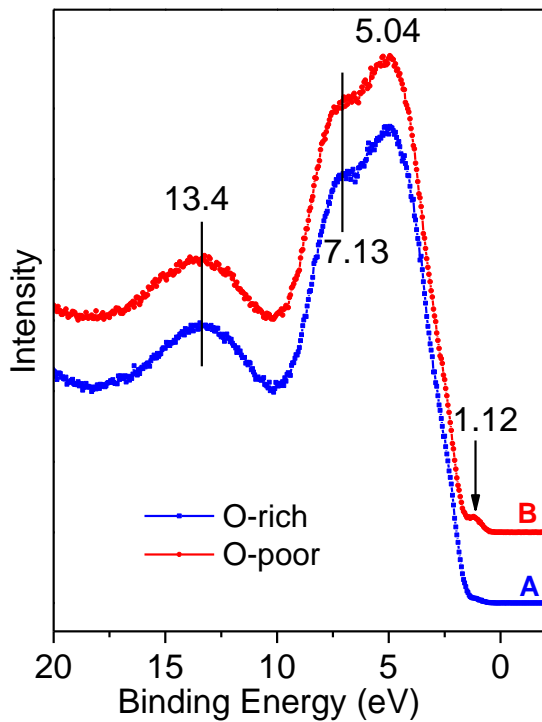


Figure 7: Valence band spectra of *O-rich* (curve A) and *O-poor* biphase  $\text{Fe}_2\text{O}_3$  (curve B). The spectra were recorded at a detection angle of  $80^\circ$  relative to the surface normal. The incident photon energy was 120 eV. Curve B has been shifted upwards along the ordinate axis; the intensities at around the abscissa's origin correspond to zero intensity of the respective spectra.

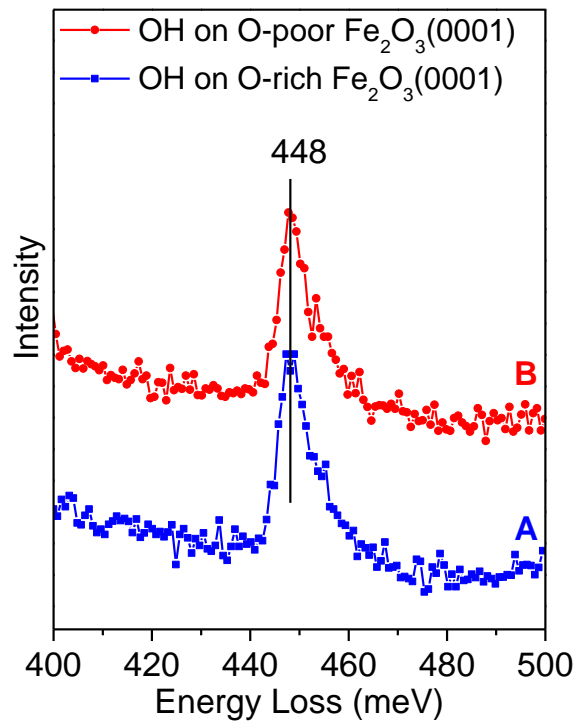


Figure 8: HREELS spectra of 1 L  $\text{H}_2\text{O}$  adsorbed on *O-rich* (curve A) and *O-poor* (curve B) biphase  $\text{Fe}_2\text{O}_3$  surfaces. Both spectra were taken in specular geometry.

The small peak located at 1.12 eV below the Fermi level in spectrum B (*O-poor*  $\text{Fe}_2\text{O}_3$ ) is obviously due to the presence of  $\text{Fe}^{2+}$ . This is consistent with a study where a similar peak at 0.9 eV was observed for a  $\text{Fe}_2\text{O}_3(0001)$  surface exposed to an Ar ion beam, which led the authors to conclude that this was a defect state [53]. The weak intensity of this peak in Figure

7 suggests that only a very small amount of oxygen is lost in the topmost layer, which is the source of most of the intensity in Figure 7. This conclusion is in line with the finding that the LEED patterns of *O-rich* and *O-poor* surfaces are nearly indistinguishable (see Figure 4).

Adsorption experiments provide additional evidence for oxygen loss below the very surface. If oxygen from the very surface layer is lost then this will create an oxygen vacancy. At pressures below  $\sim 10^{-4}$  mbar  $H_2O$  dissociates only at oxygen vacancies [9-11], where it forms two surface hydroxyls. Figure 8 compares HREEL spectra of an *O-poor* and an *O-rich* surface which were exposed to 50 L  $H_2O$  at room temperature. The  $\nu(OH)$  positions and intensities are essentially identical in both spectra, demonstrating that the hydroxyl concentrations and thus the density of vacancies giving rise to their formation were identical on both surfaces. This again leads to the conclusion that the annealing-induced oxygen loss does not occur at the very surface but below it.

We have quantified the oxygen loss using the TDS data shown in Figure 4 and find, that the oxygen desorption signal of the *O-rich* biphasic integrated up to 1000 K corresponds to roughly 30% of the oxygen in a  $FeO(111)$  monolayer. This value is the ratio of the integrated oxygen desorption signals of the *O-rich* biphasic (integration up to 1000 K) and the  $FeO(111)$  monolayer (integration up to 1100 K). The determined percentage refers to the amount of oxygen missing in *O-poor* layers relative to *O-rich* layers. There may be some error in this value since the role of oxygen uptake by the  $Pt(111)$  substrate in the  $FeO(111)$  decomposition experiment is not known. If the oxygen loss in the biphasic films was confined to the first layer, then this should lead to significant changes in the surface-sensitive data, i.e. the LEED images (Figure 5), the valence band photoelectron spectra (Figure 7), and the hydroxyl HREELS spectra (Figure 8), which is not the case. This semi-quantitative argument strongly supports

the above discussion by providing additional evidence that most of the oxygen loss must occur below that surface layer.

## 5. Summary

We have studied the initial reduction process of *O-rich* biphase Fe<sub>2</sub>O<sub>3</sub> upon annealing. Experimental techniques with different degrees of surface sensitivity were employed, supported by *ab initio* cluster calculations of excitation energies. Experimental methods with low surface sensitivity such as thermal desorption of oxygen and electronic HREELS in specular geometry reveal remarkable changes following reduction by annealing, while more surface sensitive techniques such as LEED, grazing angle valence band photoelectron spectroscopy, and vibrational spectroscopy of surface hydroxyls show only negligible differences between *O-poor* and *O-rich* surfaces, indicating that the electronic and geometric structures of the two surfaces are essentially not affected by the oxygen loss. We propose that the loss of oxygen occurs mostly in the subsurface region, at least for the degrees of reduction investigated in this study.

## Acknowledgements

This work was funded by the Deutsche Forschungsgemeinschaft (DFG) through their Sonderforschungsbereich 546 “Transition Metal Oxide Aggregates” and the Cluster of Excellence “UniCat”. We thank the Helmholtz-Zentrum in Berlin for the allocation of

synchrotron radiation beamtime at beamline UE52-PGM. One of the authors (E.B.) thanks the Alexander von Humboldt Foundation for a Senior Humboldt Grant.

## References:

- [1] W. Weiss, W. Ranke, *Surface chemistry and catalysis on well defined epitaxial iron-oxide layers*, *Prog. Surf. Sci.*, 70 (2002) 1.
- [2] A. Kay, I. Cesar, M. Grätzel, *New benchmark for water photooxidation by nanostructured  $\alpha$ -Fe<sub>2</sub>O<sub>3</sub> films*, *J. Am. Chem. Soc.*, 128 (2006) 15714.
- [3] G. Wang, W. Li, K. Jia, B. Spliethoff, F. Schüth, A. Lu, *Shape and size controlled  $\alpha$ -Fe<sub>2</sub>O<sub>3</sub> nanoparticles as supports for gold catalysts: synthesis and influence of support shape and size on catalytic performance*, *Appl. Catal., A*, 364 (2009) 42.
- [4] R.M. Cornell, U. Schwertmann, *The iron oxides: structure, properties, reactions, occurrence and uses*, WILEY-VCH Verlag GmbH & Co. KGaA, Weinheim, 2003.
- [5] P.L. Liao, E.A. Carter, *Testing variations of the GW approximation on strongly correlated transition metal oxides: hematite ( $\alpha$ -Fe<sub>2</sub>O<sub>3</sub>) as a benchmark*, *PCCP*, 13 (2011) 15189.
- [6] G. Rollmann, A. Rohrbach, P. Entel, J. Hafner, *First principle calculation of the structure and magnetic phases of hematite*, *Phys. Rev. B*, 69 (2004) 165107.
- [7] A. Kiejna, T. Pabisiak, *Surface properties of clean and Au or Pd covered hematite ( $\alpha$ -Fe<sub>2</sub>O<sub>3</sub>(0001))*, *J. Phys. Condens. Matter*, 24 (2012) 095003.
- [8] A. Barbieri, W. Weiss, M.A. Van Hove, G.A. Somorjai, *Magnetite Fe<sub>3</sub>O<sub>4</sub>(111) - surface-structure by LEED crystallography and energetics*, *Surf. Sci.*, 302 (1994) 259-279.
- [9] A. Rohrbach, J. Hafner, G. Kresse, *Ab initio study of the (0001) surfaces of hematite and chromia: influence of strong electronic correlations*, *Phys. Rev. B*, 70 (2004) 125426.
- [10] G. Ketteler, W. Weiss, W. Ranke, R. Schlögl, *Bulk and surface phases of iron oxides in an oxygen and water atmosphere at low pressure*, *PCCP*, 3 (2001) 1114.
- [11] G. Ketteler, W. Weiss, W. Ranke, *Surface structure of  $\alpha$ -Fe<sub>2</sub>O<sub>3</sub>(0001) phases determined by LEED crystallography*, *Surf. Rev. Lett.*, 8 (2001) 661.
- [12] A. Barbier, A. Stierle, N. Kasper, M.J. Guittet, J. Jupille, *Surface termination of hematite at environmental oxygen pressures: Experimental surface phase diagram*, *Phys. Rev. B: Condens. Matter*, 75 (2007) 233406.
- [13] S.K. Shaikhutdinov, W. Weiss, *Oxygen pressure dependence of the  $\alpha$ -Fe<sub>2</sub>O<sub>3</sub>(0001) surface structure*, *Surf. Sci.*, 432 (1999) L627.
- [14] X.G. Wang, W. Weiss, S.K. Shaikhutdinov, M. Ritter, M. Petersen, F. Wagner, R. Schlögl, M. Scheffler, *The hematite ( $\alpha$ -Fe<sub>2</sub>O<sub>3</sub>) (0001) surface: evidence for domains of distinct chemistry*, *Phys. Rev. Lett.*, 81 (1998) 1038.
- [15] N.G. Condon, P.W. Murray, F.M. Leibsle, G. Thornton, A.R. Lennie, D.J. Vaughan, *Fe<sub>3</sub>O<sub>4</sub>(111) termination of  $\alpha$ -Fe<sub>2</sub>O<sub>3</sub>(0001)*, *Surf. Sci.*, 310 (1994) L609.
- [16] C.H. Lanier, A.N. Chiamonti, L.D. Marks, K.R. Poepelmeier, *The Fe<sub>3</sub>O<sub>4</sub> origin of the "biphase" reconstruction on  $\alpha$ -Fe<sub>2</sub>O<sub>3</sub>(0001)*, *Surf. Sci.*, 603 (2009) 2574.
- [17] R.J. Lad, V.E. Henrich, *Structure of  $\alpha$ -Fe<sub>2</sub>O<sub>3</sub> single-crystal surfaces following Ar<sup>+</sup> ion-bombardment and annealing in O<sub>2</sub>*, *Surf. Sci.*, 193 (1988) 81-93.
- [18] N.G. Condon, F.M. Leibsle, A.R. Lennie, P.W. Murray, D.J. Vaughan, G. Thornton, *Biphase ordering of Iron oxide surfaces*, *Phys. Rev. Lett.*, 75 (1995) 1961.
- [19] Y. Tang, H. Qin, K. Wu, Q. Guo, J. Guo, *The reduction and oxidation of Fe<sub>2</sub>O<sub>3</sub>(0001) surface investigated by scanning tunneling microscopy*, *Surf. Sci.*, 609 (2013) 67-72.
- [20] C. Lemire, S. Bertarione, A. Zecchina, D. Scarano, A. Chaka, S. Shaikhutdinov, H.J. Freund, *Ferryl (Fe=O) termination of the hematite  $\alpha$ -Fe<sub>2</sub>O<sub>3</sub>(0001) surface*, *Phys. Rev. Lett.*, 94 (2005) 166101.
- [21] J. Goniakowski, F. Finoacchi, C. Noguera, *Polarity of oxide surfaces and nanostructures*, *Rep. Prog. Phys.*, 71 (2008) 016501.
- [22] J.K. Leland, A.J. Bard, *Photochemistry of colloidal semiconducting Iron oxide polymorphs*, *J. Phys. Chem.*, 91 (1987) 5077.
- [23] W. Huang, W. Ranke, R. Schlögl, *Reduction of an  $\alpha$ -Fe<sub>2</sub>O<sub>3</sub>(0001) film using atomic hydrogen*, *J. Phys. Chem. C*, 111 (2007) 2198.

- [24] M. Xue, S. Wang, K. Wu, J. Guo, Q. Guo, *Surface structural evolution in iron oxide thin films*, *Langmuir*, 27 (2010) 11.
- [25] F. Alvarez-Ramirez, J.M. Martinez-Magadan, J.R.B. Gomes, F. Illas, *On the geometric structure of the (0001) hematite surface*, *Surf. Sci.*, 558 (2004) 4.
- [26] G.J. Martin, R.S. Cutting, D.J. Vaughan, M.C. Warren, *Bulk and key surface structures of hematite, magnetite and goethite: a density functional theory study*, *Am. Mineral.*, 94 (2009) 1341.
- [27] N.C. Wilson, S.P. Russo, *Ilmenite (0001) surface investigated using hybrid density functional theory*, *Phys. Rev. B*, 84 (2011) 075310.
- [28] Z.D. Pozun, G. Henkelman, *Hybrid density functional theory band structure engineering in hematite*, *J. Chem. Phys.*, 134 (2011) 224706.
- [29] A. Barbier, A. Stierle, F. Finocchi, J. Jupille, *Stability and stoichiometry of polar oxide surfaces for varying oxygen chemical potential*, *J. Phys.: Condens. Matter*, 20 (2008) 184014.
- [30] S. Tougaard, <http://www.quases.com>.
- [31] M. Lewandowski, *Scanning tunneling microscopy study of iron oxide based model catalysts*, in: *Technische Universität Berlin, Fakultät III - Prozesswissenschaften, Berlin, 2011*.
- [32] H.-J. Freund, G. Pacchioni, *Oxide ultra-thin films on metals: new materials for the design of supported metal catalysts*, *Chem. Soc. Rev.*, 37 (2008) 2224.
- [33] R.W.G. Wyckoff, *Crystal structures*, Interscience Publishers, New York, 1965.
- [34] A. Freitag, V. Staemmler, D. Cappus, C.A. Ventrice Jr., K. Al Shamery, H. Kuhlbeck, H.-J. Freund, *Electronic surface state of NiO(100)*, *Chem. Phys. Lett.*, 210 (1993) 10.
- [35] V. Staemmler, *The cluster approach for the adsorption of small molecules on oxide surfaces*, *Top. Organomet. Chem.*, 12 (2005) 219.
- [36] H. Stoll, *private communication*.
- [37] V. Staemmler, *Note on open shell restricted SCF calculations for rotation barrier about C-C double bonds: ethylene and allene*, *Theoret. Chim. Acta*, 45 (1977) 89.
- [38] U. Meier, V. Staemmler, *An efficient first order CASSCF method based on the renormalized Fock-operator technique*, *Theoret. Chim. Acta*, 76 (1989) 95.
- [39] J. Wasilewski, *Graphical techniques in the configuration interaction approach based on pure Slater determinants*, *Int. J. Quantum Chem.*, 36 (1989) 503.
- [40] C.E. Moore, *Atomic energy levels*, *Natl. Bur. Stand, Washington*, 1971.
- [41] S. Mochizuki, *Electrical conductivity of  $\alpha$ -Fe<sub>2</sub>O<sub>3</sub>*, *Phys. Stat. Sol. (a)*, 41 (1977) 591.
- [42] B. Ouertani, J. Ouerfelli, M. Saadoun, H. Ezzaouia, B. Bessais, *Characterisation of iron oxide thin films prepared from spray pyrolysis of iron trichloride based aqueous solution*, *Thin Solid Films*, 516 (2008) 8584.
- [43] H. Ibach, D.L. Mills, *Electron energy loss spectroscopy and surface vibrations*, Academic Press, New York, 1982.
- [44] S.C. Petitto, E.M. Marsh, G.A. Carson, M.A. Langell, *Cobalt oxide surface chemistry: the interaction of CoO, Co<sub>3</sub>O<sub>4</sub> and Co<sub>3</sub>O<sub>4</sub>(111) with oxygen and water*, *J. Mol. Catal. A: Chemical*, 281 (2008) 49.
- [45] Y. Sun, L. Giordano, J. Goniakowski, M. Lewandowski, Z. Qin, C. Noguera, S. Shaikhutdinov, G. Pacchioni, H.J. Freund, *The interplay between structure and CO oxidation catalysis on metal-supported ultrathin oxide films*, *Angew. Chem. Int. Ed.*, 49 (2010) 4418.
- [46] M.P. Seah, W.A. Dench, *Quantitative electron spectroscopy of surfaces: A standard data base for electron inelastic mean free paths in solids*, *Surf. Interface Anal.*, 1 (1979) 2-11.
- [47] B. Götz, D.B. Popović, D.E. David, J. Michl, P. Swiderek, *Depth and Angular Profiles of Inelastic Low-Energy Electron Scattering in Condensed Molecular Samples*, *The Journal of Physical Chemistry B*, 110 (2006) 5480-5485.
- [48] S. Andersson, B.N.J. Persson, T. Gustafsson, E.W. Plummer, *Vibrational excitation cross-sections for adsorbed CO*, *Solid State Commun.*, 34 (1980) 473-476.
- [49] B.N.J. Persson, H. Ibach, *Inelastic scattering of slow electrons from adsorbed CO*, *Surf. Sci.*, 99 (1980) 283-288.

- [50] A. Fujimori, M. Saeki, N. Kimizuka, M. Taniguchi, S. Suga, *Photoemission satellites and electronic structure of Fe<sub>2</sub>O<sub>3</sub>*, *Phys. Rev. B*, 34 (1986) 7318.
- [51] T. Fuji, F.M.F. de Groot, G.A. Sawatzky, F.C. Voogt, T. Hibma, *In situ XPS analysis of various iron oxide films grown by NO<sub>2</sub>-assisted molecular beam epitaxy*, *Phys. Rev. B*, 59 (1999) 3195.
- [52] W. Temesghen, P.M.A. Sherwood, *Analytical utility of valence band X-ray photoelectron spectroscopy of iron and its oxide with spectral interpretation by cluster and band structure calculations*, *Anal. Bioanal. Chem.*, 373 (2002) 601.
- [53] R.L. Kurtz, V.E. Henrich, *Surface electronic structure and chemisorption on corundum transition-metal oxides:  $\alpha$ -Fe<sub>2</sub>O<sub>3</sub>*, *Phys. Rev. B*, 36 (1987) 3413.

## Tables and captions:

Table 1: Results of the cluster calculations for the lowest excitation energy (in eV) for a Fe<sup>3+</sup> ion (d<sup>5</sup> configuration) in different oxide environments

Crystal	FeO	FeO	FeO	Fe <sub>2</sub> O <sub>3</sub>
R(Fe-O) / Å	2.16	2.08	2.02	2.08/1.96
bulk	3.58	3.37	3.00	3.42
surface	3.54	3.29	2.89	3.69

Table 2a: Lowest energy levels (in eV) for the Fe<sup>2+</sup> ion (d<sup>6</sup> configuration), bulk

Crystal	FeO	FeO	FeO	Fe <sub>2</sub> O <sub>3</sub>
R(Fe-O) / Å	2.16	2.08	2.02	2.08/1.96
<sup>5</sup> T <sub>2g</sub> ( <sup>5</sup> D) <sup>a)</sup>	0.00	0.00	0.00	0.00
<sup>5</sup> E <sub>g</sub> ( <sup>5</sup> D)	0.99	1.19	1.44	1.15
<sup>3</sup> T <sub>1g</sub> ( <sup>3</sup> P)	2.08	1.93	1.72	1.93

a) The designations of the atomic states are given in parentheses.

Table 2b: Lowest energy levels (in eV) for the Fe<sup>2+</sup> ion (d<sup>6</sup> configuration), surface

Crystal	FeO	FeO	FeO	Fe <sub>2</sub> O <sub>3</sub>
R(Fe-O) / Å	2.16	2.08	2.02	2.08/1.96
<sup>5</sup> D <sup>b)</sup>	0.00 (2)	0.00 (2)	0.00 (2)	0.00 (1)
	0.22 (1)	0.21 (1)	0.22 (1)	0.41 (1)
	0.39 (1)	0.43 (1)	0.50 (1)	0.43 (1)
	1.16 (1)	1.40 (1)	1.61 (1)	1.09 (2)
<sup>3</sup> P	2.17	1.98	1.77	2.64

b) The degeneracies of the components of the atomic <sup>5</sup>D state in the different crystal fields are given in parentheses. For the <sup>3</sup>P state only the average value of its three components is presented.